First Results from Alcator C-MOD

I.H. Hutchinson, R. Boivin, F. Bombarda*, P. Bonoli,
S. Fairfax, C. Fiore, J. Goetz, S. Golovato, R. Granetz,
M. Greenwald, S. Horne, A. Hubbard, J. Irby, B. LaBombard,
B. Lipschultz, E. Marmar, G. McCracken, M. Porkolab,
J. Rice, J. Snipes, Y. Takase, J. Terry, S. Wolfe,
C. Christensen, D. Garnier, M. Graf, T. Hsu, T. Luke,
M. May[†], A. Niemczewski, G. Tinios, J. Schachter, J. Urbahn
Plasma Fusion Center
Massachusetts Institute of Technology
Cambridge, MA 02139
November, 1993

*Visitor from ENEA Frascati, Italy.
[†]Johns Hopkins University.

First Results from Alcator C-MOD.

I.H. Hutchinson, R. Boivin, F. Bombarda*, P. Bonoli, S. Fairfax, C. Fiore, J. Goetz,

S. Golovato, R. Granetz, M. Greenwald, S. Horne, A. Hubbard, J. Irby, B. LaBombard,

B. Lipschultz, E. Marmar, G. McCracken, M. Porkolab, J. Rice, J. Snipes, Y. Takase,

J. Terry, S. Wolfe, C. Christensen, D. Garnier, M. Graf, T. Hsu, T. Luke, M.May†,

A. Niemczewski, G. Tinios, J. Schachter, J. Urbahn

Plasma Fusion Center, MIT, Cambridge, MA, U.S.A.

Abstract

Early operation of the Alcator C-MOD tokamak is surveyed. Reliable operation, with plasma current up to 1 MA, has been obtained, despite the massive conducting super-structure and the associated error fields. However, vertical disruptions are not slowed by the long vessel time-constant. With pellet fueling, peak densities up to 9×10^{20} m^{-3} have been attained and 'Snakes' are often seen. Initial characterization of divertor and scrape-off layer is presented and indicates approximately Bohm diffusion. The edge plasma shows a wealth of MARFE-like phenomena, including a transition to detachment from the divertor plates with accompanying radiative divertor regions. Energy confinement generally appears to exceed the expectations of Neo-Alcator scaling. A transition to ohmic H-mode has been observed. ICRF experiments have demonstrated good power coupling, in agreement with theory.

*Visitor from ENEA Frascati, Italy,

†Johns Hopkins Univesrity.

I Introduction

Alcator C-MOD[1], the third high-field compact tokamak in the Alcator line, has been operating tokamak plasmas since May 1993. Its design capability includes toroidal field, $B_T = 9$ T, plasma current I_p up to 3 MA, in plasmas with major radius $R = 0.67$ m, minor radius $a = 0.21$ m, with elongation up to $\kappa = 1.8$. Divertor operation can be either into its closed, baffled, divertor chamber or to open flat plates. The magnetic configuration is rather similar to that presently envisaged for the International Thermonuclear Experimental Reactor, ITER, except that it is about a factor of ten smaller.

The high particle-, current- and power-densities characteristic of such compact tokamaks lead to edge conditions that are in many respects comparable to those expected in ITER, and offer the opportunity to investigate so-called dissipative divertor operation, in which the power scraped off into the divertor is exhausted through a combination of neutral and radiative processes rather than through plasma conduction direct to the divertor plates.

Alcator C-MOD offers excellent port access to the plasma for diagnostic and heating purposes. Its present complement of diagnostics includes full magnetics for equilibrium reconstruction, electron temperature profiles from electron cyclotron emission (ECE), density profiles from a ten-channel CO_2 laser interferometer, ion temperature profiles from high-resolution x-ray doppler measurements, neutron emission, and fast neutral particle analysis, various spectroscopic measurements such as visible bremsstrahlung, H_α arrays, and vacuum ultraviolet impurity measurements, bolometer arrays, and x-ray and UV tomography. In addition, detailed edge, scrape-off-layer and divertor diagnosis based on probes and spectroscopy is available.

The primary auxiliary heating method in the short term is ICRF, and two transmitters are available, providing a total 4 MW at 80 MHz. Thus far, experiments have concentrated on plasma coupling studies using a movable monopole antenna. Good power coupling into high density plasmas has been obtained, with loading resistance in the range of 5 to 15 Ω,

in reasonable agreement with the theoretical calculations.

So far the magnetic field has been limited to about 5.3 T awaiting power systems upgrades that will enable full-field operation next year. Even so, plasma currents up to 1 MA have been obtained, and durations over 1 second. Peak electron densities up to 9×10^{20} m^{-3}, and temperatures up to $T_e = 2.6$, $T_i = 1.6$ keV have been achieved. Energy confinement is observed to exceed Neo-Alcator scaling.

In section II we review some MHD and operational characteristics of the plasma. Section III discusses divertor experiments, section IV the confinement results, and section V the first ICRF coupling studies.

II MHD and Operation

A unique feature of the design of Alcator C-MOD is its thick stainless-steel vacuum vessel and structure. For reasons of mechanical strength, these have no insulating breaks and thus constitute 'shorted turns' on the ohmic transformer and the eddy currents induced in the structure are therefore very large. Modelling indicates that up to 1 MA flows during the initiation of the plasma when the loop-voltage is relatively high. Low voltage (5 − 8 volts per turn) startup is used to minimize the stray fields from the structure but these poloidal fields are still of order 0.1 T. Since they cannot be modelled at the 1 mT level observed to be necessary for plasma breakdown, the approach adopted is to reconstruct the fields in the plasma region using the magnetic flux loop measurements and then to null out the fields by adjusting the coil currents. Rather detailed reconstructions of the vacuum fields are obtained in the process[2]. Figure 1 shows an example.

The thirteen poloidal field coils in Alcator C-MOD are controlled by 10 independent power supplies. Each coil serves simultaneously to provide ohmic drive, equilibrium fields and plasma shape control, as part of the combined system. Their currents are controlled using a fast hybrid feedback control system[3] which operates linearly upon the diagnostic signals but whose control matrix can be switched up to 500 times during the pulse at

3

intervals as small as 2 ms. During the precharge phase prior to plasma initiation, the feedback serves to bring the currents to prescribed values, with fine-scale control of actual field parameters important for breakdown, e.g. the horizontal field B_R.

During plasma initiation and current rise, and into the main plasma phase, feedback is transferred to relevant plasma parameters. In addition to the familiar radial and vertical plasma position and current, the shape parameters presently under feedback control include the radial and vertical position of the x-points and the clearance between the separatrix and the inner wall limiter surface. Using this combination, 'slot-divertor' and shaped divertor configurations with swept strike-point have been routinely produced, as discussed in section IV.

Figure 2 shows the evolution of various of the plasma parameters during a typical shot. The current, radial position, and inner clearance (gap) are well controlled during the flat-top. The density has been controlled over a factor of more than 10 by gas puffing. In this case it increases throughout the shot, with the electron temperature decreasing in response. Radiated power is a small fraction of the ohmic input, the spike at 0.82 s is a deliberate injection of scandium for impurity transport studies. The Z_{eff} from visible bremsstrahlung suffers uncertainties of about 30% due to profile effects but the value is very close to one at the higher densities, and is consistent with plasma resistivity.

Figure 3 shows a reconstruction, using the EFIT code[4], of a 1 MA plasma equilibrium. This shape is typical also, of many other plasmas, including that of Fig. 2.

A major aspect of any tokamak control is the problem of disruptions. Alcator C-MOD's vacuum vessel has a time-constant for poloidal fields of about 10-20ms. It is therefore of interest to observe whether this relatively long time-constant has any mitigating effects on the disruptive instability; especially, does it slow the current ramp rate to a level that might reduce the extreme forces associated with the disruption-induced currents? We observe that if the plasma is well controlled vertically, the current ramp rate following even an almost complete energy quench is slow, greater than 10ms, and that the

plasma generally reheats. (It should be noted, however, that these are mostly fairly low β_p and high safety factor shots.) In the more usual case, when a Vertical Displacement Event (VDE) occurs, either as a result or as a cause of a disruption, the current can fall from essentially its flat-top level to a small fraction of that level in as little as 0.5 ms, much shorter than the vessel time-constant. Current decay rates as large as 1 MA/ms, and vertical velocities up to 1 km/s have been observed.

During the VDE's the 'halo' currents flowing on open field lines have been measured using shunts attached to the divertor plates. Over 10kA has been observed in plates covering one tenth of the toroidal circumference, in events starting at 0.4 MA plasma current, when the motion is toward the divertor. This would translate to more than 25% of the plasma current total flowing in the halo, consistent with observations on other tokamaks[5].

Pellet injection has been used to fuel to the highest densities. Deuterium and Lithium pellet injectors are available, and both have been seen to induce the "snake" phenomenon, which was first seen on JET[6]. The localized density perturbation, as much as 50% of local density in the snake feature, is extremely long-lived, and several examples of snakes surviving through multiple sawteeth have been observed in Alcator C-MOD on both the density interferometer and x-ray imaging diagnostics. Figure 4 shows an example. It is believed that the snake marks the location of the $q = 1$ surface, and the temporal behavior of its radial position therefore yields information on the evolution of the q-profile during the sawtooth crash. In figure 4, the snake radius shrinks by about 50% at each crash, and slowly expands back during the sawtooth ramp. The simplest interpretation of this data, taking the safety factor profile to be approximated by a parabola near the axis, would indicate that the value of $1 - q_0$ decreases by a factor of 4 at the crash. Such a result, if correct, rules out the possibility that the axial safety factor, q_0, remains well below unity at the crash, but also indicates that elimination of the $q = 1$ surface does not occur.

5

III Divertor

The Alcator C-MOD lower divertor has been operated both as a shaped divertor, with oblique impact of the separatrix into the divertor plates and as a 'slot' divertor, with the separatrix running almost parallel to the plates, so as to provide a long field-line length in which to test dissipative divertor concepts. Two typical configurations are illustrated in Fig. 5.

The divertor is instrumented with 'flush-mount' electric probes embedded in the divertor structure, also shown in Fig. 5. Although the detailed interpretation of such probes in terms of density and temperature is uncertain because of the lack of an established theory of their operation, they provide semi-quantitative information about the plasma profile in the divertor. We find that in the slot divertor configuration, plasma is observed all the way down the outer divertor plate surface, which is in the common-flux SOL. When the separatrix intersects the plate, in a shaped divertor configuration, the probes map out the profile across the separatrix.

Figure 6(a) shows a typical profile of ion current collected on the outer probe array plotted versus a flux surface label that corresponds to the distance into the SOL at the plasma midplane. Observations of the shot-to-shot variation in the location of the peak ion current collection suggest that the magnetic reconstruction of the divertor strike point is accurate to approximately +/-2 mm using this mapped coordinate. We generally observe that the gradient scale length of the plasma profile in the private-flux region is much shorter than in the common-flux region.

A fast-scanning Langmuir probe has been used to obtain the profiles of electron density and temperature in the SOL close to the entrance to the divertor (see Fig. 5). An example of density and temperature profiles, mapped to the SOL coordinate at the plasma midplane, is shown in Fig. 6(b,c). Although the precise location of the last-closed flux surface (LCFS) is slightly uncertain in this figure, both the density and temperature profiles exhibit a steepening of the gradient scale length as the last-closed flux surface is approached. The

6

density e-folding lengths for this discharge are 3 mm near the LCFS and 8 mm further into the SOL. The temperature profile exhibits corresponding e-folding lengths of 4.6 mm and 13 mm. From these measurements, a radial particle diffusion coefficient in the range of 0.14-0.24 m^2s^{-1} is estimated for the common flux zone. This is comparable to a Bohm diffusion value of 0.2 m^2s^{-1}.

It may be noted that the sharp gradients near the LCFS yield a very short power e-folding length of approximately 1.5 mm, while further into the SOL the power e-folding length increases to 4 mm. The parallel heat flux to the probe, which may be considered as an estimate of the maximum heat flux which could flow into the divertor region, can be estimated from the temperature and saturation current. Using a sheath heat transmission coefficient of 7, the peak parallel heat flux to the probe for this discharge is approximately 180 MW/m^2.

A notable feature of much of the early operation of the tokamak has been the presence of a MARFE[8], a strongly radiating, poloidally localized high-density region at the plasma periphery. The most graphic illustration of this phenomenon has been through a toroidally viewing TV camera with a CIII (466.0 nm) line filter. The MARFE also shows up strongly on other spectroscopic diagnostics such as UV diodes, bolometers, and H_α and CIII detectors. With toroidal field direction such that the ion ∇B drift is upwards, the MARFE region is typically located at the inboard side (small major radius) of the tokamak, from 0.1 to 0.3 m above the midplane. Figure 7 shows an example. This MARFE impedes the fuelling of the plasma through gas puffing, and thus limits the maximum attainable density. Strong gas puffing into a discharge with a MARFE in this location frequently leads to a detached plasma, where the power conducted to the divertor plates is reduced essentially to zero, and all of the input power is removed by radiation and charge-exchange. In this event, the TV image shows that the MARFE region spreads poloidally and moves in radially about 5 cm, so that a shell of radiation, well inside the separatrix, is observed.

Under some circumstances, the MARFE is observed to move rapidly ($\sim$ 2 ms) down

to the shaped divertor x-point region. This leads to sharp decreases in molybdenum and carbon influxes from the inner wall, and decreases in radiation in the main plasma, coincident with increases in radiated power from the shaped divertor region.

With the ion ∇B drift direction downward, the MARFE location was observed to move to well below the midplane, just above the shaped divertor, still on the inboard side. Fuelling through gas puffing has been extended in this configuration, and main plasma central chord average densities, $\bar{n}_e > 3 \times 10^{20}$ m^{-3} have been achieved. A possible interpretation is that the growth of the MARFE to a fully detached plasma is restrained by the increased power which flows to it when the MARFE is near or in the divertor.

When strong gas puffing is applied to a plasma where the MARFE is already in the divertor, the power flow to the divertor in the region of the strike points is suddenly extinguished. During the transition to this new state, illustrated in Fig. 8, at the strike points there is a decrease in plasma density (by a factor of 7), temperature (by a factor of 2 or more) and conducted power (factor of 20). This is simultaneous with a rearrangement of the radiation in the divertor.

Analysis of data from the bolometer arrays, the H$_\alpha$ diagnostics, and the TV, viewing the shaped divertor, indicate that the radiating region, which was located at the inner divertor, moves to affect both the inner and outer divertors. It is possible that this localized radiating region moves slightly inside the separatrix as well. We hypothesize that those flux lines which pass through the radiating region are efficently drained of power flow just before that power reaches the divertor plates. However, at points intercepted by common flux field lines one scrape-off length or more outside the separatrix, there is constant or somewhat increased power flow. The main plasma density increases rapidly, but in ~ 100 ms reaches a new steady state. The radiated power from the main chamber increases (from 200 kW to 270 kW) but reaches a new steady state value that is still less than 30% of the total power. Although bearing some resemblance to radiative divertor observations on JET[9] and MARFEs on Asdex Upgrade[10], the apparent preferential extinction of the

8

power near the separatrix strike-points is a new feature of considerable interest. Much further investigation of this phenomenon is planned.

IV Ohmic Confinement

Alcator C-Mod operates in a unique parameter range for study of the relationship between ohmic and auxiliary heated confinement scalings. When operated at low densities ($\lesssim$ 2×10^{20} m^{-3}), its combination of small size and high current leads to large ratios of the L-mode to the Neo-Alcator confinement predictions.

Our ohmic confinement results were expected, on the basis of ohmic scaling in Alcator C and other tokamaks, to follow Neo-Alcator scaling with saturation at the higher densities. However, early results do not confirm this expectation. Plasmas show energy confinement often significantly higher than Neo-Alcator. Overall, confinement scales more strongly with plasma current than with density in a manner resembling L-mode. This result must be seen as preliminary at the moment because, for this data from early in the operating life of C-Mod, wall condition is suspect for at least some of the shots analyzed, the diagnostic set, while performing admirably, is still incomplete, and some problems of consistency between measurements and among analysis techniques remain to be resolved.

Shots for the confinement data base were chosen as far as possible to be steady state, non-disruptive, and sawtoothing. Stored plasma energy was calculated by three independent methods. In the first, density and temperature profiles were volume integrated; density measurements came from the CO_2 interferometer, electron temperature from ECE, ion temperature from Doppler broadening x-ray lines of argon impurities. The second method employed was to extract the stored energy from the full MHD equilibrium reconstructions calculated by the EFIT code. Because of the relatively low β_p, about 0.25, the fractional uncertainty in the reconstructed energy is considerable. The last method used was analysis of plasma diamagnetism. Despite the difficulties with this method also at low β_p, careful construction and calibration of diamagnetic loops and compensation coils has allowed de-

9

termination of stored energy from this diagnostic for our ohmic plasmas. RMS noise on the calculated energy is about 5 kJ and agreement with the equilibrium measurement is typically good to about 20-30% in stored energy.

Figure 9 shows the measured τ_E plotted against current, I_p and density, $\bar{n}_e$. The characteristic Alcator scaling of confinement time with density is virtually absent. But the current dependence of the confinement is very evident. Figure 10(a) plots the measured τ_E against neo-Alcator[11], $\tau_{na} = 0.192 \times 10^{-20} \bar{n}_e R^{2.04} a^{1.04} \kappa^{1/2}$ s . The dashed line with slope equal to one shows where data that agrees exactly with the scaling would lie. The lowest values of τ are consistent with neo-Alcator, but a great deal of the data lies a factor of two above the line. Figure 10(b) plots the measured τ_E against L-mode scaling, in this case the ITER89-P scaling[12], $\tau_E = 0.048(I_p/MA)^{0.85} R^{1.2} a^{0.3} \kappa^{0.5} (n_e/10^{20})^{0.1} B^{0.2} (m_i/m_p)^{0.5}$ $(P/MW)^{-0.5}$ s. Though there is a great deal of scatter, the L-mode scaling with its strong I_p dependence, seems to match the data better than neo-Alcator with its dominant density dependence.

At somewhat reduced toroidal field ($B_t \sim 3$ T), transition to ohmic H-mode has been observed. The density ($\bar{n}_e \sim 10^{20} \text{m}^{-3}$), and power per unit plasma surface area ($p \sim 1$ MW/7 m^2) at the transition correspond to $p/(B_t \bar{n}_e) \sim 0.05\ 10^{-20}$ MW m T^{-1}, consistent with recent threshold scalings[13]. Substantial transient increases in energy and particle confinement time have been observed. We have also obtained transitions to ohmic H-mode at $B_T = 5.3$ T, with threshold power density $p/(B_t \bar{n}_e) \sim 0.03\ 10^{-20}$MWmT^{-1}. At the higher field, frequent ELMs are observed throughout the H-phase, while the lower field cases are ELM-free.

V ICRF

In ICRF experiments on Alcator C[14], severe degradation of antenna power handling and plasma heating were observed at high densities ($\bar{n}_e \gtrsim 2 \times 10^{20}$ m^{-3}), and consequently there arose some question as to whether coupling of ICRF heating power is really possible at the high densities typical in Alcator. Our ICRF experiments thus far on Alcator C-MOD have focussed on coupling questions using a monopole (single current strap) antenna. This antenna is movable so as to vary its position with respect to the plasma for a wide variety of plasma shapes. (Future dipole antennas will be fixed because of the difficulty of sustaining the larger disruption forces). The monopole antenna is made of silver plated inconel, centrally grounded, fed from both ends, and has a Titanium-Carbide coated double-layer Faraday shield. We have found that high power densities can in fact be coupled even with the present monopole antenna.

Detailed theoretical calculations of the expected loading resistance have been carried out with the slab-geometry, full-wave code FELICE[15]. A comparison of the experimental results with the code is shown in Figure 11. Because of the fairly large density scrape-off width and relatively long parallel wavelength, good coupling can be obtained with the antenna as far as 5 cm from the separatrix. We also observe that a larger gap from the separatrix to the outboard limiter is advantageous in reducing impurity influx.

Although major heating experiments await later campaigns with two dipole antennas, we have coupled up to 0.75 MW peak power. This corresponds to an antenna power density of $\gtrsim 10$ MW m^{-2}, comparable to the highest achieved on a tokamak.

Acknowledgements

References

[1] I. H. Hutchinson, *Proceedings of the IEEE 13th Symposium on Fusion Engineering*, Knoxville, TN, edited by M. Lubell, M. Nestor, and S. Vaughan (IEEE New York, 1990), volume 1, p13.

[2] I. Hutchinson, R. Boivin, P. Bonoli, C. Fiore, J. Goetz, S. Golovato, R. Granetz, M. Greenwald, S. Horne, A. Hubbard, J. Irby, B. LaBombard, B. Lipschultz, E. Marmar, M. Porkolab, J. Rice, J. Snipes, Y. Takase, J. Terry, S. Wolfe, C. Christensen, D. Garnier, M. Graf, T. Hsu, D. Jablonski, C. Kurz, T. Luke, J. Murphy, A. Niemczewski, P. O'Shea, J. Reardon, J. Schachter, P. Stek, G. Tinios, C. Tsui, J. Urbahn, and Y. Wang, European Physical Society Conference on Plasma Physics and Controlled Fusion, Lisboa, Portugal, July 1993, postdeadline paper, MIT report PFC/CP-93-1, See National Technical Information Service document no. DE94001565, price code: A01. Copies may be ordered from the NTIS, Springfield, Virginia 22161.

[3] P.F. Isoz, J.B. Lister, and P. Marmillod, *Fusion Technology*, (proceeding of the 16th SOFT conference, London, 1990) edited by B. E. Keen, M. Huguet, and R. Hemsworth, Elsevier, New York, (1991).

[4] L. L. Lao, H. St.John, R. D. Stambaugh, A. G. Kellman, and W. Pfeiffer, Nucl. Fusion **25**, 1611 (1985).

[6] E.J. Strait, L.L. Lau, J.L. Luxon, E.E. Reis, Nucl. Fusion **31**, 527 (1991).

[7] A. Weller, A. D. Cheetham, A. W. Edwards, R. D. Gill, A. Gondhalekar, R. S. Granetz,

J. Snipes, and J. A. Wesson, Phys. Rev. Lett. **59**, 2303 (1987).

[8] B. Lipschultz, J. Nucl. Mater. **145-147**, 15 (1987).

[9] G. Janeschitz, S. Clement, N. Gottardi, M. Lesourd, J. Lingertat, C. Lowry, G. Radford, G. Saibene, M. Stamp, D. Summers, A. Taroni, P.R. Thomas, G. Vlases, Contr. Fusion and Plasma Physics (Proc. 19th Europ. Conf., Innsbruck, 1992), Vol. 16C, Part II, 727.

[10] V. Mertens, K. Büchl, W. Junker, F. Mast, M. Schittenhelm, M. Bessenrodt-Weberpals, A. Field, Ch. Fuchs, O. Gehre, O. Gruber, A. Herrmann, G. Haas, A. Kallenbach, H. Kastelewicz, M. Kaufmann, W. Köppendörfer, M. Laux, G. Lieder, J. Neuhauser, F. Ryter, H. Salzmann, W. Sandmann, K.-H. Steuer, A. Stäbler, H. Zohm, ASDEX Upgrade Team, Contr. Fusion and Plasma Physics (Proc. 20th Europ. Conf., Lisboa, 1993), Vol. 17C, Part I, 267.

[11] R. R. Parker, M. Greenwald, S. C. Luckhardt, E. S. Marmar, M. Porkolab, and S. M. Wolfe, Nucl. Fusion, **25**, 1127 (1985).

[12] *ITER Physics Design Guidelines*, compiled by N. A. Uckan and ITER physics group, IAEA Vienna, 1990.

[13] F. Ryter, O. Gruber, K. Büchl, A.R. Field, C. Fuchs, O. Gehre, A. Herrmann, M. Kaufmann, W. Köppendörfer, F. Mast, H. Murmann, J.-M. Noterdaeme, G.V. Pereverzev, H. Zohn, Contr. Fusion and Plasma Physics (Proc. 20th Europ. Conf., Lisboa, 1993), Vol. 17C, Part I, I-23.

[14] T. D. Shepard, C. L. Fiore, F. S. McDermott, R. R. Parker, M. Porkolab, Phys. Fluids B 3, 1657 (1991).

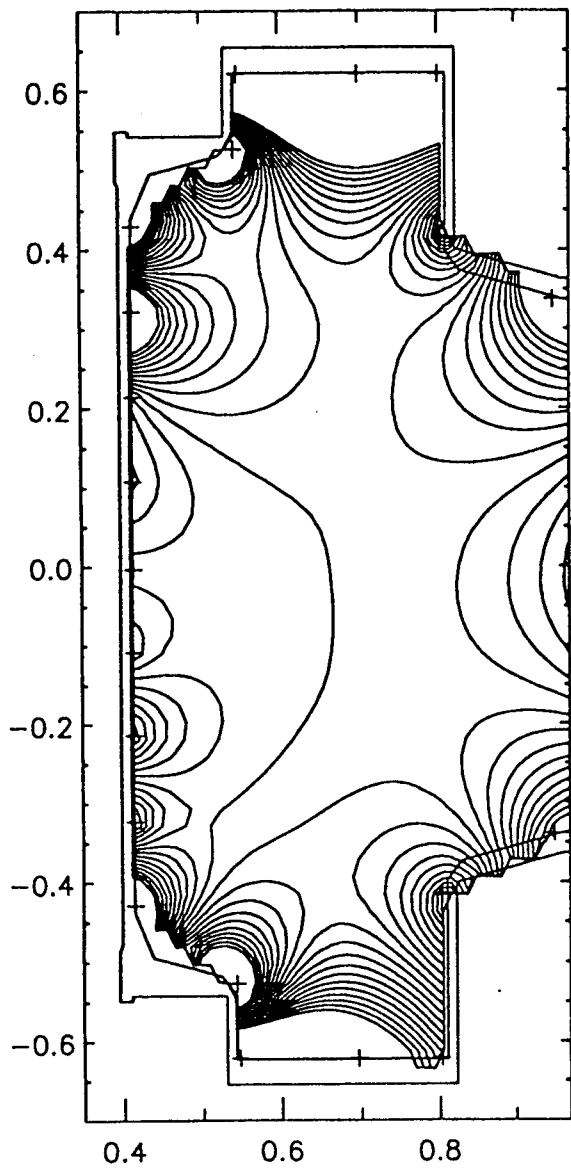[15] M. Brambilla, Nucl. Fusion, **28**, 549 (1988).

Figure Captions

Figure 1. Reconstructed vacuum field null at the time of plasma ionization. Contours of poloidal flux are spaced by 0.001 Wb. The stray fields have been cancelled to less than 1 mT over much of the vessel.
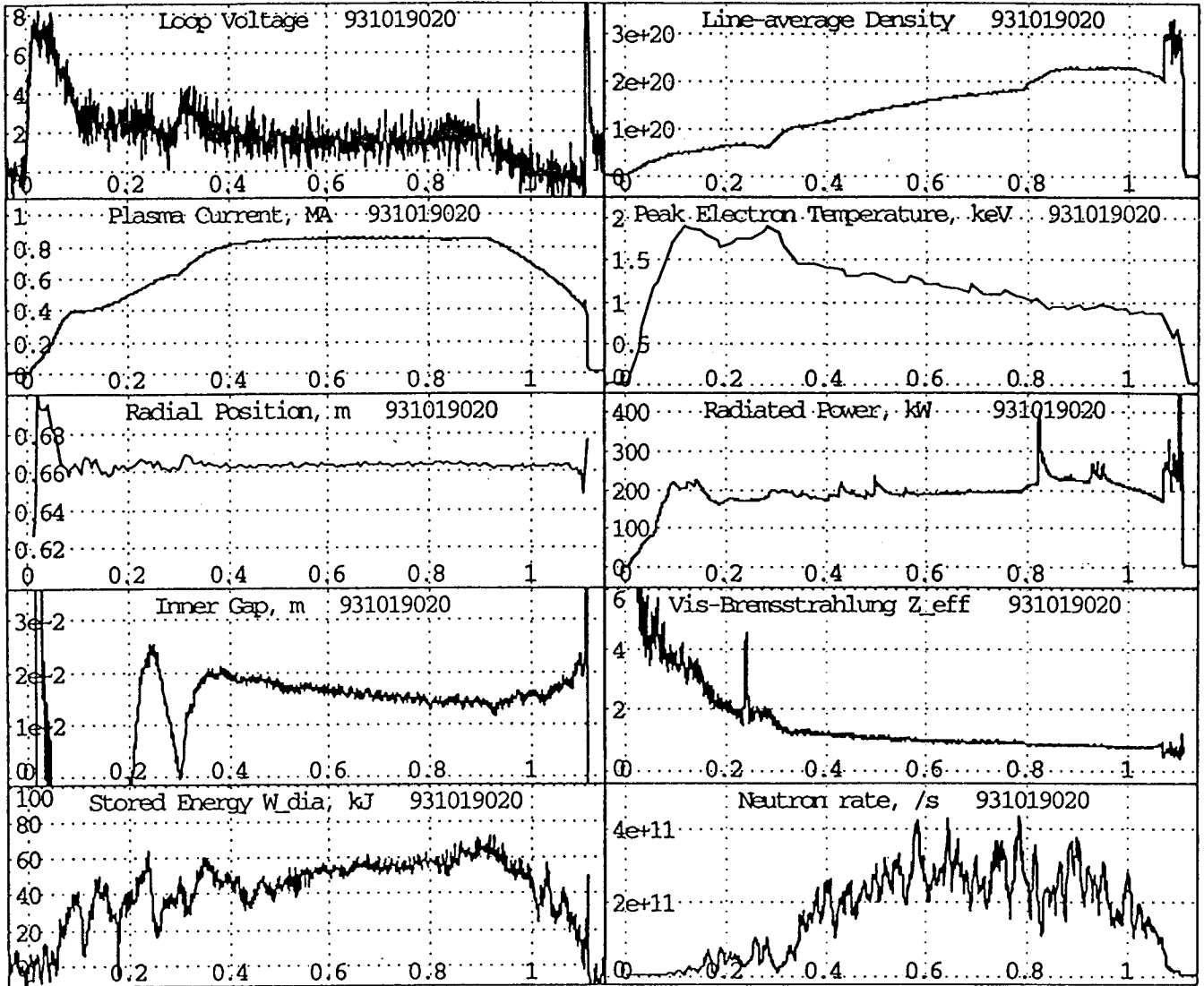
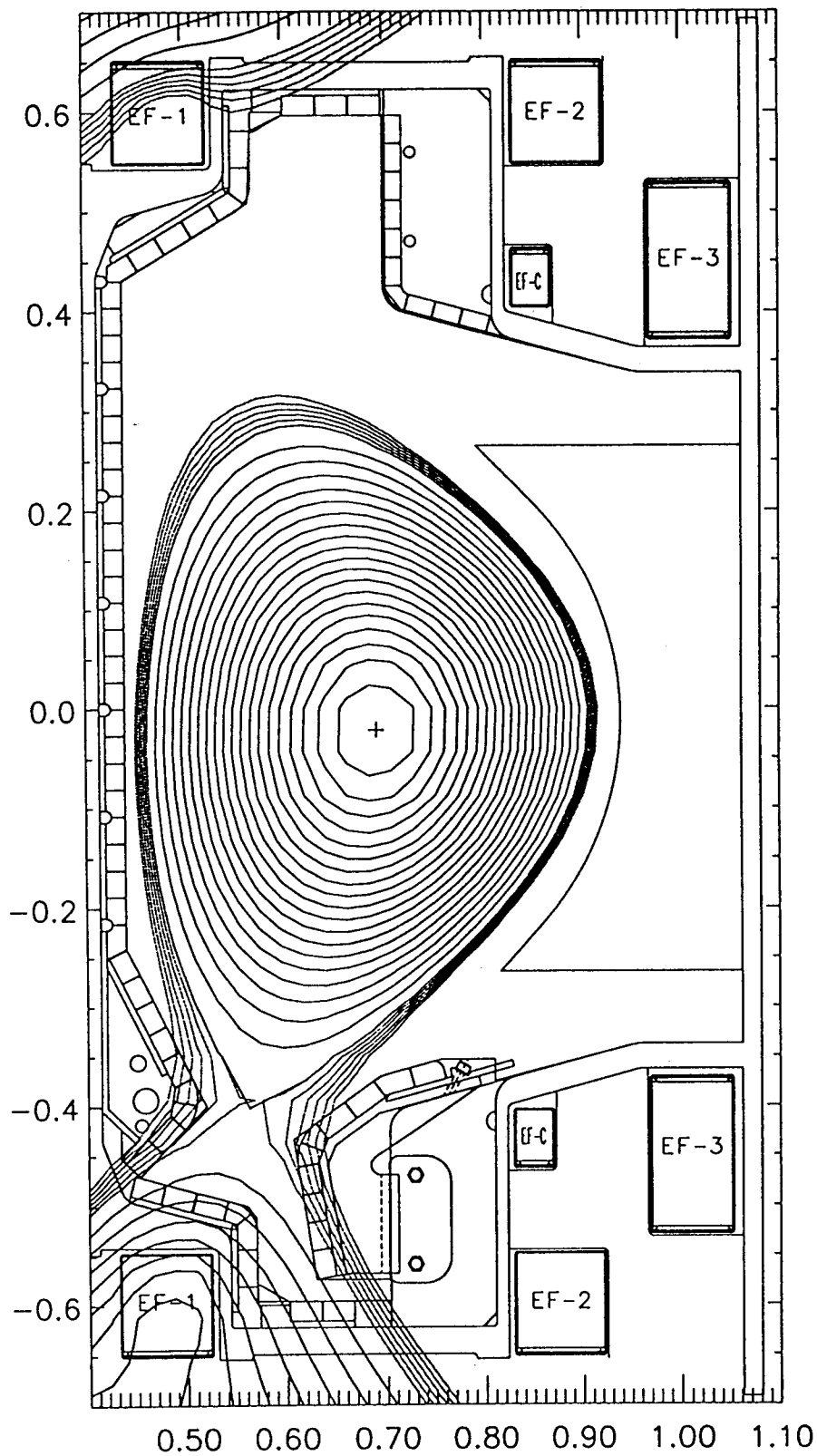Figure 2. Time evolution of various parameters during a typical shot.

Figure 3. EFIT reconstruction of a 1 MA plasma equilibrium. The poloidal field coils combine to provide ohmic drive, equilibrium, and shaping, producing a well diverted plasma.
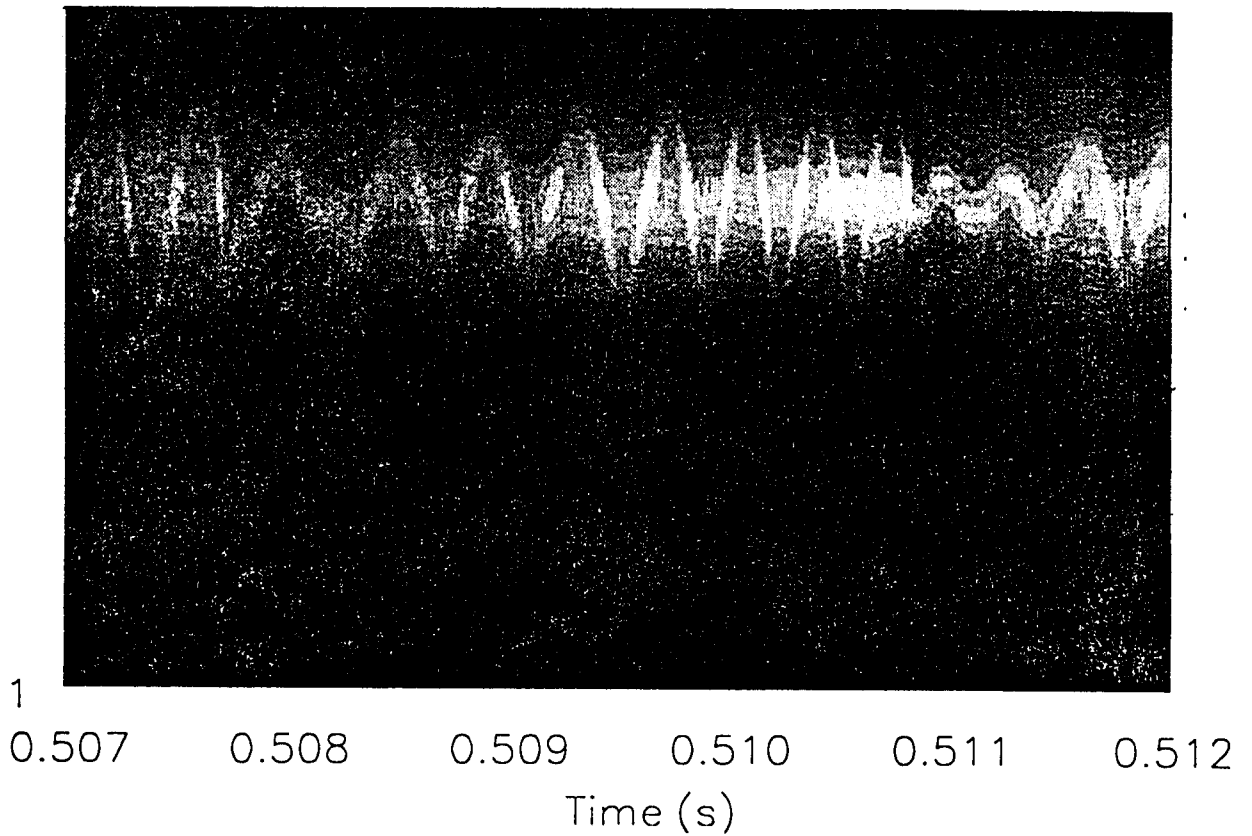
Figure 4. View of a "snake", using a high-resolution x-ray camera. Shading indicates x-ray intensity as a function of chord minor radius (vertical scale) and time (horizontal scale). The maximum snake diameter is about 15 cm.

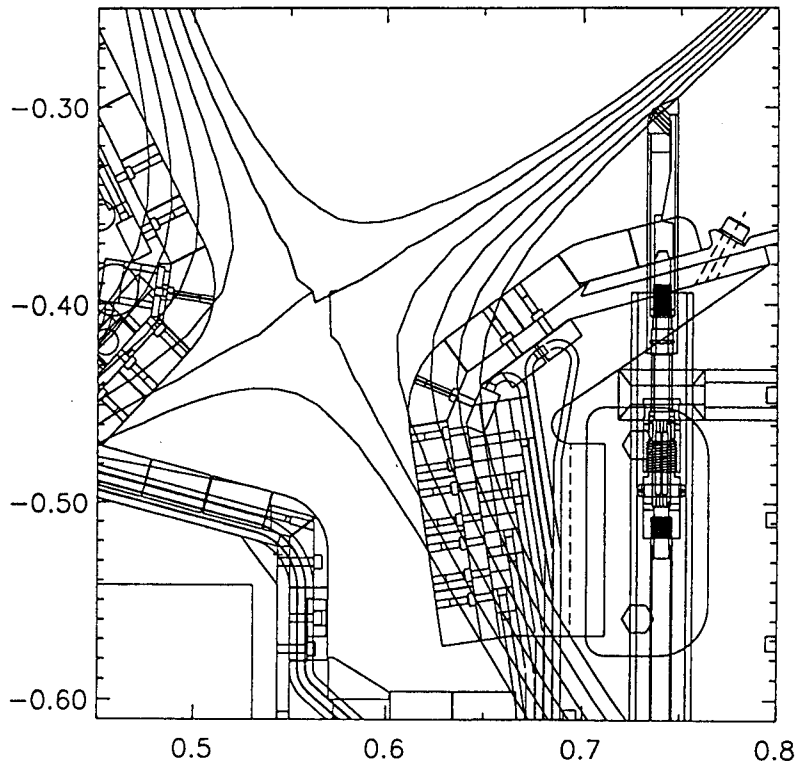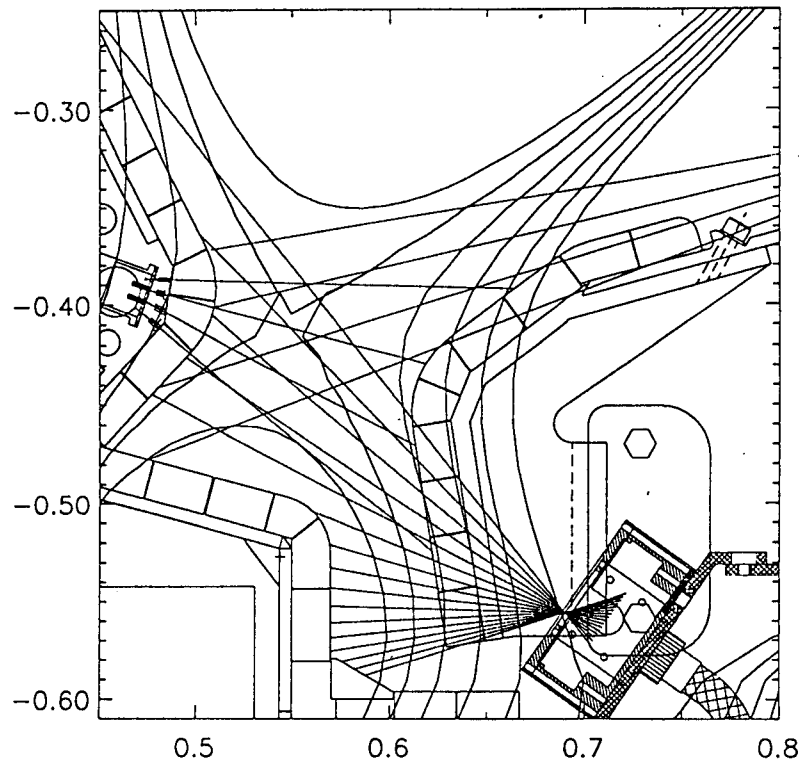Figure 5. The divertor configuration of Alcator C-MOD. (a) A shaped divertor magnetic configuration, with the layout of the probe diagnostics. (b) A 'slot' divertor magnetic configuration, with the layout of some of the bolometric diagnostics.

Figure 6. Divertor and scrape-off profiles. (a) Divertor-plate ion-saturation current, (b) SOL density, (c) SOL temperature, all mapped to radial position of their flux-surface at the plasma midplane.

Figure 7. TV view of the plasma in CIII light during a MARFE. The view is tangential, with the inner cylinder to the right and the outer wall of the vacuum vessel to the left. Thus, the region of strong emission (the MARFE region) is on the inboard side and well above the midplane. The positions of some of the internal components in this view are also indicated, but it should be noted that they are *behind* the emitting plasma column.

Figure 8. Transition to detached divertor. (a) The density at the divertor plate in the strike-point and common-flux regions are measured by Langmuir probes. (b) Radiated power along two chords in the divertor. Chord 1 views just above the x-point and chord 2 just below.

Figure 9. Energy confinement time versus (a) plasma current, (b) line-average density.

14

Figure 10. Comparison of measured energy confinement time with (a) Neo-Alcator and (b) ITER89-P scalings.

Figure 11. Experimentally measured antenna coupling resistance (squares) and predictions of full-wave modeling (solid line) as functions of the antenna radial position. Measured density profile was used up to the outboard limiter ($R = 93\,\text{cm}$) and a vacuum gap is assumed from this radius to the antenna position.

931020026   Contours: 0.001Wb
0.006s.

Figure 1. Reconstructed vacuum field null at the time of plasma ionization. Contours of poloidal flux are spaced by 0.001 Wb. The stray fields have been cancelled to less than 1 mT over much of the vessel.

Figure 2. Time evolution of various parameters during a typical shot.

Figure 3. EFIT reconstruction of a 1 MA plasma equilibrium. The poloidal field coils combine to provide ohmic drive, equilibrium, and shaping, producing a well diverted plasma.

18

Figure 4. View of a "snake", using a high-resolution x-ray camera. Shading indicates x-ray intensity as a function of chord minor radius (vertical scale) and time (horizontal scale). The maximum snake diameter is about 15 cm.

0.730s.

0.240s.

Fig. 5(b)

Figure 5. The divertor configuration of Alcator C-MOD. (a) A shaped divertor magnetic configuration, with the layout of the probe diagnostics. (b) A 'slot' divertor magnetic configuration, with the layout of some of the bolometric diagnostics.

Divertor Probe Currents

Fig. 6(a)

SOL Density Profile

Fig. 6(b)

SOL Temperature Profile

Fig. 6(c)

Figure 6. Divertor and scrape-off profiles. (a) Divertor-plate ion-saturation current, (b) SOL density, (c) SOL temperature, all mapped to radial position of their flux-surface at the plasma midplane.

21

Figure 7. TV view of the plasma in CIII light during a MARFE. The view is tangential, with the inner cylinder to the right and the outer wall of the vacuum vessel to the left. Thus, the region of strong emission (the MARFE region) is on the inboard side and well above the midplane. The positions of some of the internal components in this view are also indicated, but it should be noted that they are *behind* the emitting plasma column.
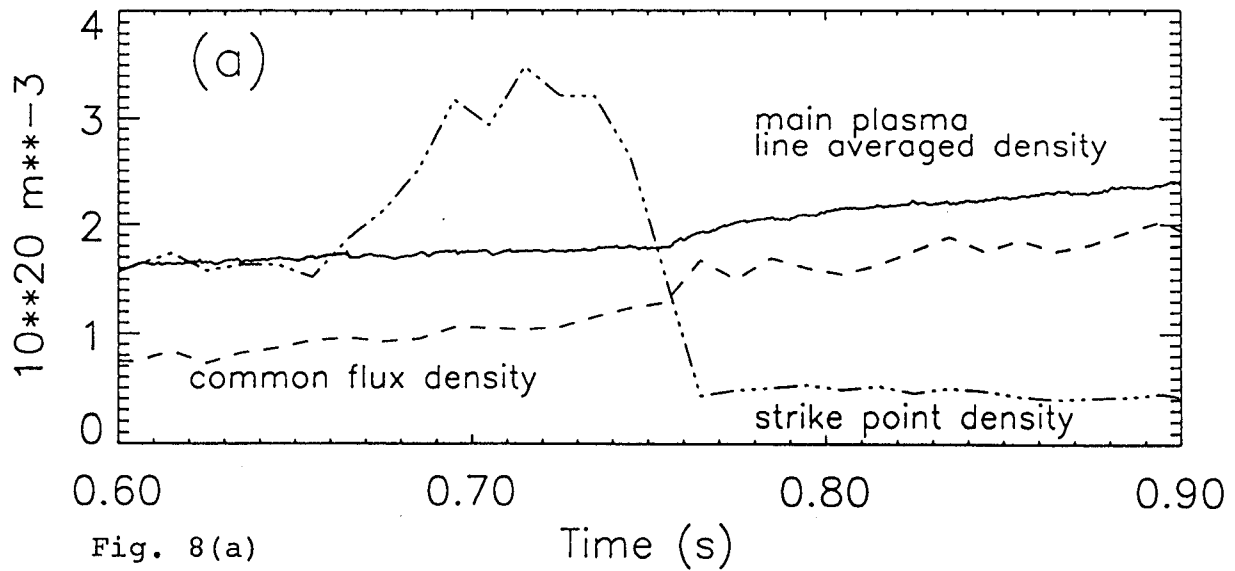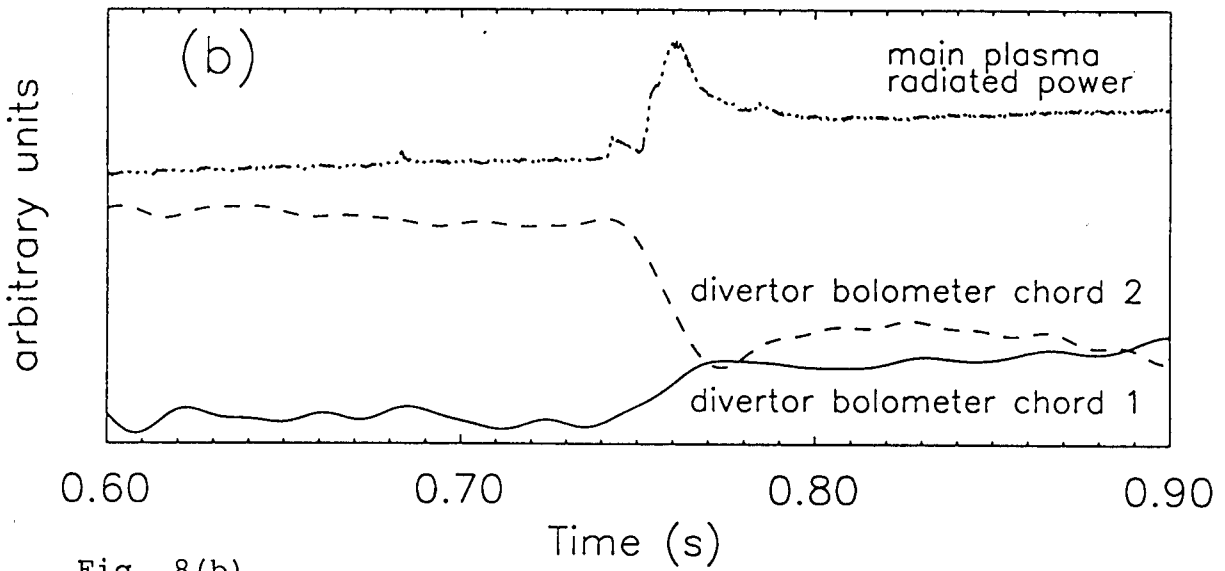
Fig. 8(a)

Fig. 8(b)

Figure 8. Transition to detached divertor. (a) The density at the divertor plate in the strike-point and common-flux regions are measured by Langmuir probes. (b) Radiated power along two chords in the divertor. Chord 1 views just above the x-point and chord 2 just below.
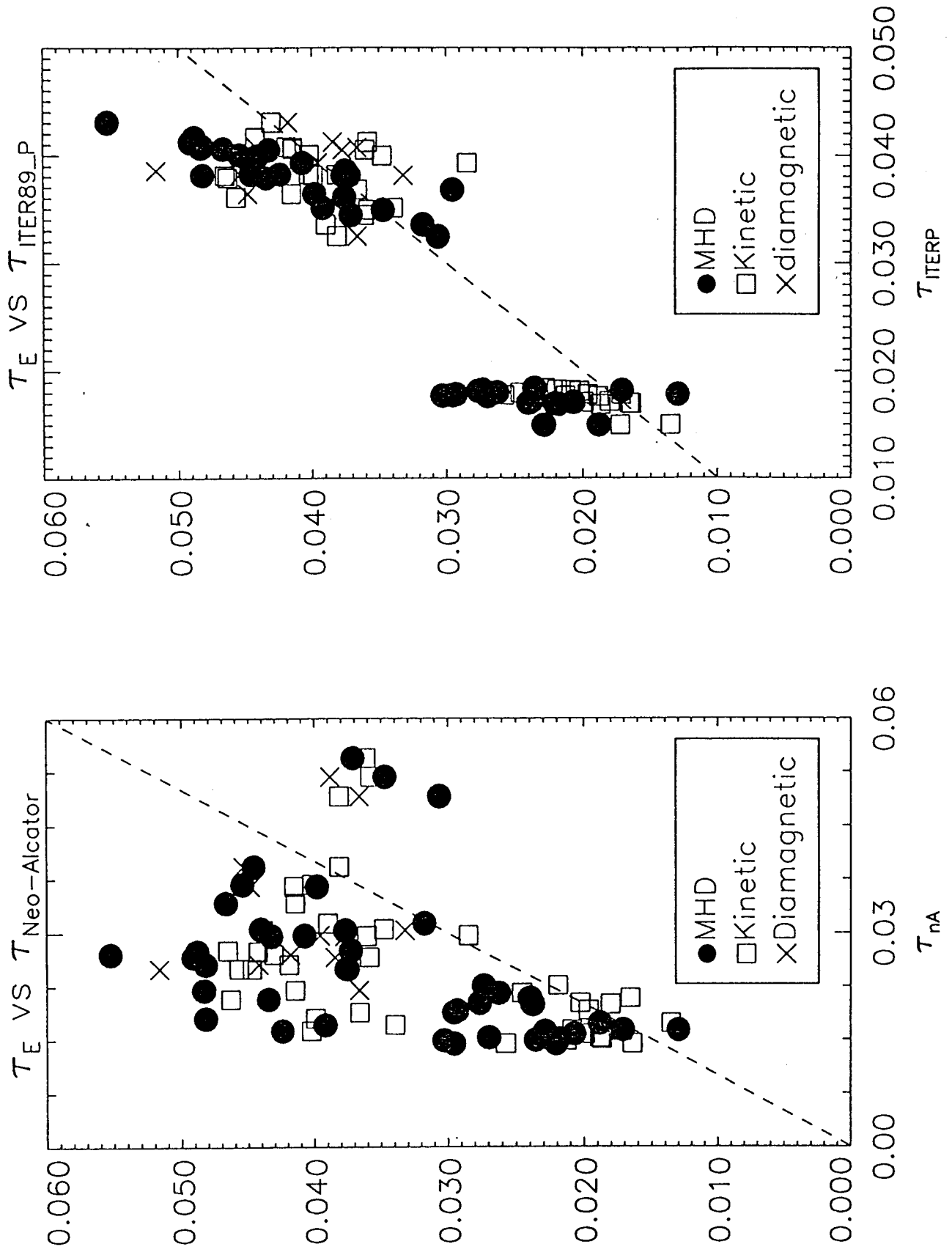
Figure 9. Energy confinement time versus (a) plasma current, (b) line-average density.
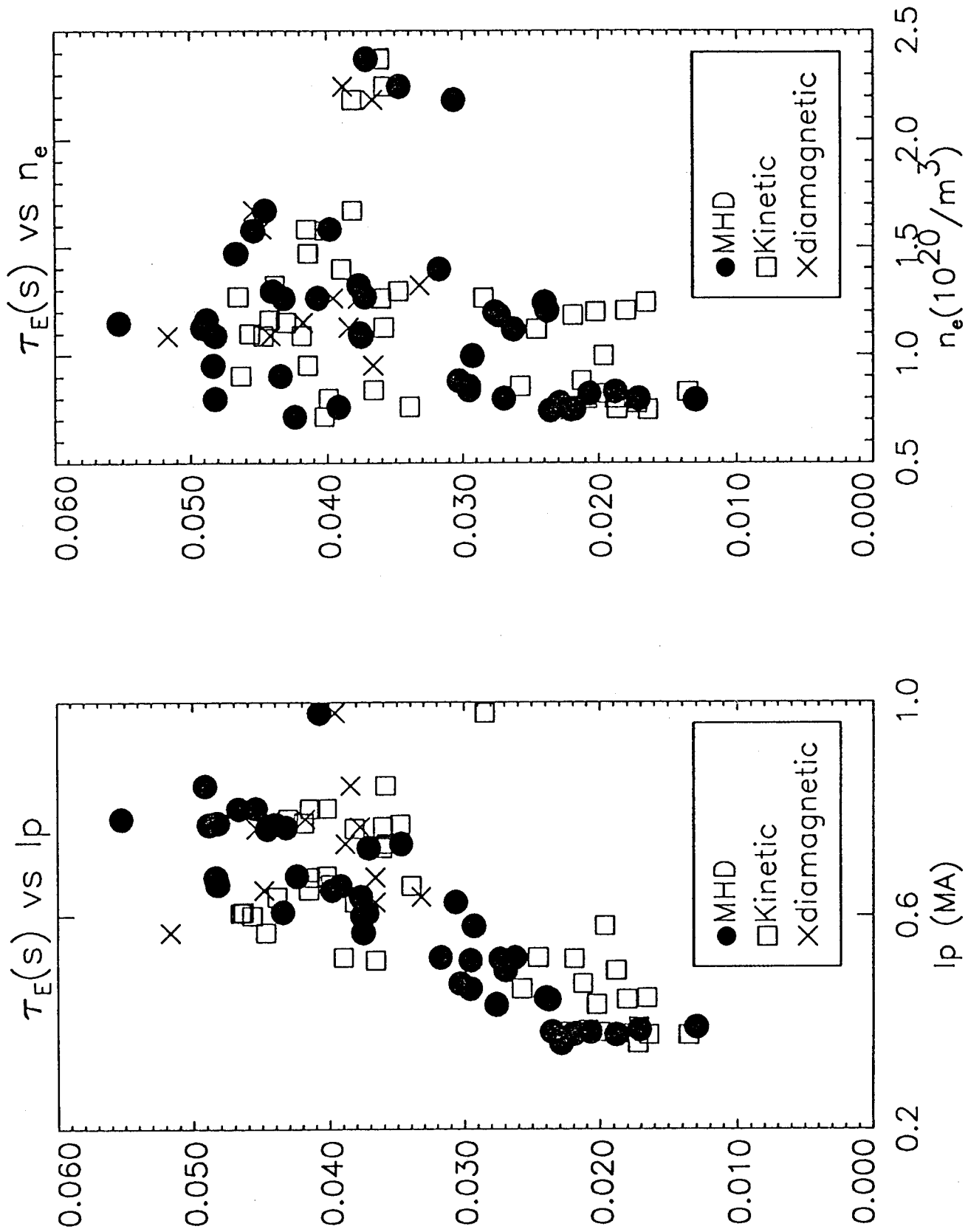
Figure 10. Comparison of measured energy confinement time with (a) Neo-Alcator and
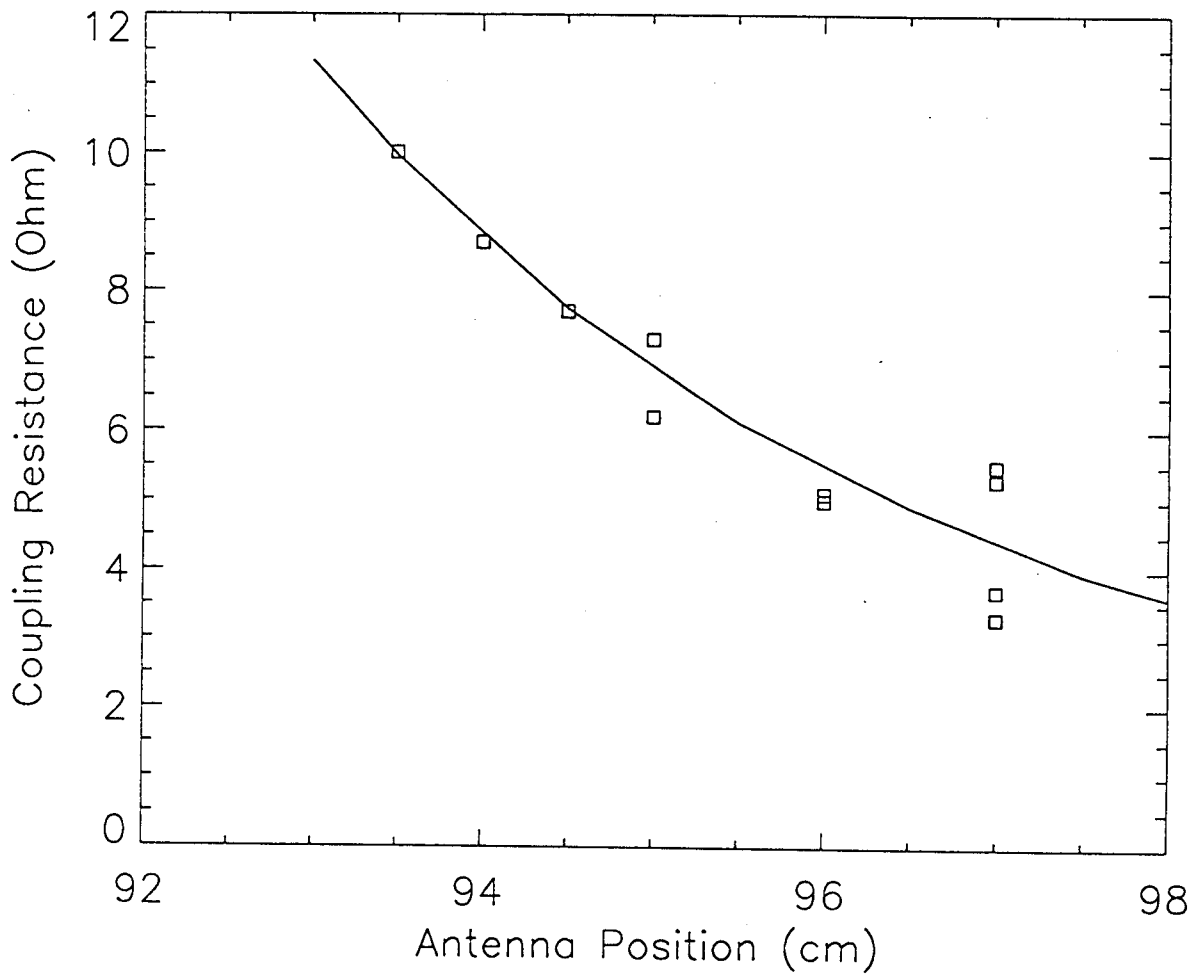
(b) ITER89-P scalings.

Figure 11. Experimentally measured antenna coupling resistance (squares) and predictions of full-wave modeling (solid line) as functions of the antenna radial position. Measured density profile was used up to the outboard limiter ($R = 93\,\mathrm{cm}$) and a vacuum gap is assumed from this radius to the antenna position.